Available online at www.sciencedirect.com
ScienceDirect
Lithos 95 (2007) 87–102
LITHOS
www.elsevier.com/locate/lithos

In situ synchrotron-radiation XRF study of REE phosphate dissolution in aqueous fluids to 800 °C

Christian Schmidt [a,*], Karen Rickers [a,b], Donald H. Bilderback [c], Rong Huang [c]

[a] GeoForschungsZentrum Potsdam, Telegrafenberg, Potsdam D-14473, Germany
[b] Hamburger Synchrotronstrahlungslabor at Deutsches Elektronensynchrotron, Notkestrasse 85, Hamburg D-22603, Germany
[c] Cornell High Energy Synchrotron Source, Cornell University, 281 Wilson Laboratory, Ithaca, New York 14853, USA

Received 19 October 2005; accepted 7 July 2006
Available online 15 September 2006

Abstract

The temporal evolution of the concentrations of La, Ce, Pr, Nd, Sm, Gd, Y, Pb, Th, and U in the fluid during dissolution of synthetic $LaPO_4$ monazite, natural monazite, and xenotime in aqueous HCl±NaCl solutions was studied in situ at temperatures from 25 to 800 °C and pressures to about 2 GPa using hydrothermal diamond-anvil cells and synchrotron-radiation XRF analyses. Constant (within error) La concentrations in the fluid were attained in less than 50 min at temperatures ≥300 °C and in less than 90 min at 200 °C. At 100 °C, the time required to reach a constant La concentration varied with the HCl molality from less than 3 h at 5.1 *m* HCl to ≥11 h at 1 *m* HCl. The experiments indicate a significantly lower mobility of Y, Gd, and Th compared to that of the LREE, particularly La, over a large range of crustal *P*–*T* conditions if controlled by interaction of monazite with acidic and chloridic fluids. The corresponding change in the REE pattern is in close agreement with literature reports on natural monazites, which underwent greisenization or sericitization. The Th/Pb ratio in the fluid increased with temperature and HCl concentration, but was far below the Th/Pb ratio in the monazite even at 600 °C and 2 GPa. The experimental results imply that monazites leached in acidic and chloridic fluids are characterized by a strong enrichment of Th relative to the LREE and Pb.
© 2006 Elsevier B.V. All rights reserved.

Keywords: Rare-earth phosphate–aqueous fluid interactions; Dissolution kinetics; REE patterns; Th/Pb ratios; In situ SR-XRF analysis; Hydrothermal diamond-anvil cells

1. Introduction

The rare-earth phosphates xenotime (Y,HREE)PO_4 and particularly monazite (LREE,Th)PO_4 are common accessory minerals in the continental crust, where they occur in sedimentary, igneous, and low- to very high-grade metamorphic rocks. Monazite is the principal ore of Th (Boatner, 2002) and one of the main REE ore minerals, whereas xenotime is of lower economic significance (Möller, 1989). Monazite and xenotime are widely used for U–Th–Pb geochronology (e.g., Harrison et al., 2002). Additionally, monazite–xenotime and monazite–garnet equilibria are applicable as geothermometers (e.g., Gratz and Heinrich, 1997; Andrehs and Heinrich, 1998; Pyle et al., 2001) for metamorphic rocks.

Monazite and xenotime are chemically quite durable under most crustal conditions, but can react with and precipitate from aqueous fluids. Monazite in granites is altered

* Corresponding author. Tel.: +49 331 2881406; fax: +49 331 2881402.
E-mail address: hokie@gfz-potsdam.de (C. Schmidt).

0024-4937/$ - see front matter © 2006 Elsevier B.V. All rights reserved.
doi:10.1016/j.lithos.2006.07.017

by greisen fluids, sericitization, and chloritization (Cesbron, 1989; Poitrasson et al., 1996, 2000), whereas xenotime is apparently more resistant to hydrothermal alteration (Broska et al., 2005). Hydrothermal formation of monazite and, less frequently, of xenotime was reported from a variety of geologic settings, e.g., Alpine-type fissures, porphyry tin, copper, and molybdenum deposits, gold–quartz veins, and skarns (Cesbron, 1989; Gieré, 1996 and references therein). Monazite was found as daughter mineral in fluid inclusions in eclogite veins (Philippot and Selverstone, 1991). Monazites from metamorphic rocks can show fluid-induced recrystallization and overgrowths (Seydoux-Guillaume et al., 2003). Occurrences of authigenic monazite in sediments were reported by Read et al. (1987) and Evans et al. (2002). These observations suggest that rare-earth phosphate–fluid reactions can result in a higher crustal mobility of the LREE compared to that of Y and the HREE. This is supported by speciation calculations (Haas et al., 1995), which indicate that chloride complexes with the LREE are more stable at elevated temperatures and pressures than the corresponding HREE complexes.

Thus, the interaction of aqueous fluids with monazite is likely one of the major factors controlling the LREE and Th geochemistry of crustal waters (Poitrasson et al., 2004). Knowledge about these processes is also crucial for the risk assessment of nuclear waste storage in geological repositories, for which ceramics with monazite structure are being seriously considered as an actinide matrix (e.g., Ewing, 2001; Poitrasson et al., 2004). The growing interest in monazite–fluid interaction is reflected by the increasing number of publications on this subject during the last 10 years. In U–Th–Pb geochronology, recent studies showed that lead diffusion appears to be a subordinate process for the age resetting of monazite even at granulite-facies temperatures (e.g., Cherniak et al., 2004). Fluid-induced resetting of monazite was discussed on the basis of petrological observations (e.g., Braun et al., 1998) and was demonstrated experimentally (Teufel and Heinrich, 1997; Seydoux-Guillaume et al., 2002). Much more is now known about the solubility and the leaching behavior of monazite in aqueous fluids at temperatures between 23 and 150 °C and a pressure of 1 atm (e.g., Liu and Byrne, 1997; Oelkers and Poitrasson, 2002; Poitrasson et al., 2004; Cetiner et al., 2005). For higher temperatures and pressures, very few and, in part, preliminary data are available (Ayers and Watson, 1991; Devidal et al., 1998; Poitrasson et al., 2004; Ayers et al., 2004). A major reason for this is that experiments on mineral solubility in aqueous fluids become considerably more difficult with increasing pressure and temperature. Much smaller fluid volumes must be used at high pressures, which limits the analytic feasibilities and usually results in an incomplete and less accurate determination of the parameters required to derive solubility data particularly for complex systems with incongruent solubility. Analyses of the fluid after quenching from high temperatures are not representative for the actual fluid composition at the run conditions if precipitation and back reactions between fluid and minerals occurred during cooling (Walther and Orville, 1983; Manning and Boettcher, 1994). A partial solution of these problems is the in situ determination of the fluid composition at high pressures and temperatures. For elements with $Z>20$, this is feasible using modified hydrothermal diamond-anvil cells and SR-XRF (synchrotron-radiation X-ray fluorescence) analyses (Schmidt and Rickers, 2003). In the study presented here, we applied this experimental technique to investigate chemical interactions of monazite and xenotime with aqueous fluids to lower crustal P–T conditions and to explore the strengths of this in situ technique, but also its limitations for improvements in future experiments.

2. Experimental procedure

The experiments were conducted using hydrothermal diamond-anvil cells (HDAC) designed for in situ SR-XRF experiments to 2 GPa and to 800 °C (Bassett et al., 1993; Schmidt and Rickers, 2003). The lower anvil of these cells has a cylindrical recess (Fig. 1a), which permits collection of the fluorescence signal at 90° to the incident beam (Bassett et al., 2000; Schmidt and Rickers, 2003). This configuration minimizes the background in the spectra from elastic and Compton scattering and thus optimizes the signal to noise ratio. Two cells were used: HDAC-2 with a recess depth of 35 μm and HDAC-3 with a recess depth of 85 μm. Because of the deeper recess and thus the larger excitation volume, the detector signal was about 2.4 times higher when HDAC-3 was utilized, which reduced the lower limits of detection by a factor of about 0.7.

A single monazite or xenotime crystal (30 to 80 μm in diameter) and aqueous fluid were loaded into the sample chamber of the cell. The solids were synthetic hydrothermally grown pure $LaPO_4$ monazite, natural monazite from Kakola, Turku, Finland (Suominen, 1991), or xenotime from Ibitiara City, Bahia, Brazil. The compositions of the natural samples are given in Table 1. These crystals were transparent, had no optically visible solid inclusions in the selected grains, showed no or only faint chemical zoning in back scattered electron images, and there was very little compositional difference between individual grains. The fluids were aqueous HCl solutions. In addition, NaCl was present at concentrations below 0.2 *m* HCl (*m* denotes moles of solute per kg of solvent). The initial solution/solid weight ratios were about 70:1 (>20:1 and

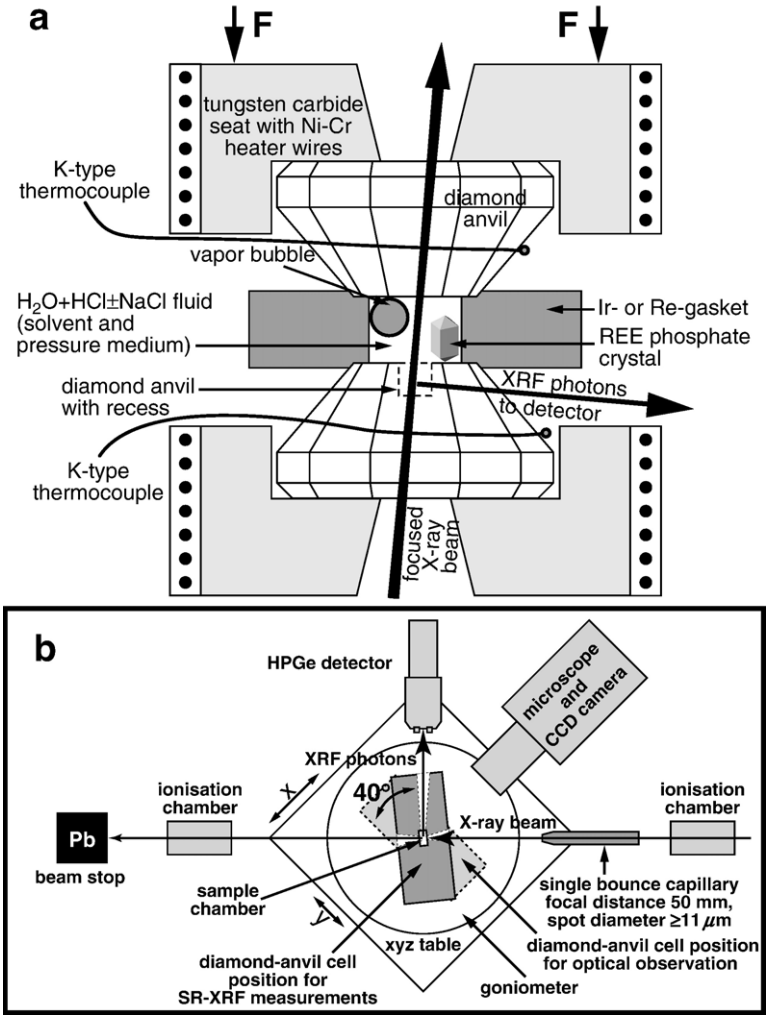


Fig. 1. Setup of the REE phosphate leaching experiments using a pink beam and a single-bounce capillary for beam focusing. Adapted from Schmidt and Rickers (2003). a) Details of the hydrothermal diamond-anvil cell designed for the in situ analysis of fluids at high pressures and temperatures using SR-XRF analyses. If a collimated (unfocused) polychromatic beam was used, the phosphate was placed in a recess cut into the gasket to keep the crystal in contact with the fluid but out of the path of the X-ray beam (cp. Fig. 1 in Schmidt and Rickers, 2003). b) Schematic diagram showing the experimental configuration at beamline L at HASYLAB/DESY.

<100:1) in the experiments in which $LaPO_4$ or xenotime was used, and 10:1 to 20:1 in the Kakola monazite leaching experiments.

Before the sample chamber was sealed, an air bubble was allowed to grow by controlled leaking of the fluid until the desired liquid–vapor ratio (fluid bulk density) was approximately attained. During this process and during fluid transfer into the sample chamber, a portion of the water evaporated. Therefore, the actual HCl concentration in the fluid after sealing was determined cryometrically from measurements of the ice melting temperature in the presence of vapor $T_{m(I+L+V\rightarrow L+V)}$. For the system H_2O+HCl, the following equation was fitted to tabulated data from various sources (Gmelin, 1968; Wolf et al., 1981) and using an eutectic temperature of −74.7 °C at 23 wt.% HCl (Gmelin, 1968):

$$\Delta = 370121(X_{HCl})^5 - 54002(X_{HCl})^4 + 14105(X_{HCl})^3 + 1288(X_{HCl})^2 + 195.6(X_{HCl}) - 0.01 \quad (1)$$

where Δ is the freezing point depression (Δ=0.01 °C − $T_{m(I+L+V\rightarrow L+V)}$ [°C]). Eq. (1) is valid for $0 \leq X_{HCl} \leq 0.1286$. At low X_{HCl}, this approach would result in large errors, because the uncertainty in determining $T_{m(I+L+V\rightarrow L+V)}$, which was about ±0.1 to ±0.2 °C, becomes significant. Therefore, 2 mol NaCl per kg H_2O were added to the 0.1 and the $1{\cdot}10^{-5}$ *m* HCl

Table 1
Electron microprobe analyses of the natural monazite and xenotime samples used for the dissolution experiments

Oxide	Weight % (standard deviation in parentheses)		Element	Element concentration normalized to 16 oxygens		Relative element concentration	
	Monazite	Xenotime		Monazite	Xenotime	Monazite, relative to Ce	Xenotime, relative to Y
P_2O_5	29.43 (0.3)	33.18 (0.22)	P	3.931	3.920	2.275	1.277
CaO	1.06 (0.25)	0.01 (0.01)	Ca	0.182	0.002	0.105	0.001
SiO_2	0.55 (0.15)	0.17 (0.04)	Si	0.088	0.023	0.051	0.008
Y_2O_3	0.66 (0.28)	41.35 (0.41)	Y	0.056	3.070	0.032	1
La_2O_3	12.43 (0.74)	0.01 (0.01)	La	0.721	0.000	0.417	0.000
Ce_2O_3	29.97 (0.99)	0.02 (0.02)	Ce	1.729	0.001	1	0.000
Pr_2O_3	3.25 (0.19)	0.01 (0.02)	Pr	0.186	0.001	0.108	0.000
Nd_2O_3	11.97 (0.92)	0.22 (0.05)	Nd	0.677	0.011	0.392	0.004
Sm_2O_3	2.08 (0.22)	0.59 (0.12)	Sm	0.113	0.028	0.066	0.009
Gd_2O_3	1.28 (0.16)	5.61 (0.31)	Gd	0.067	0.261	0.039	0.085
Tb_2O_3	0.07 (0.05)	1.22 (0.05)	Tb	0.004	0.056	0.002	0.018
Dy_2O_3	0.13 (0.12)	7.08 (0.09)	Dy	0.007	0.318	0.004	0.104
Ho_2O_3	0.03 (0.03)	1.32 (0.05)	Ho	0.002	0.059	0.001	0.019
Er_2O_3	0.07 (0.05)	3.71 (0.08)	Er	0.004	0.163	0.002	0.053
Yb_2O_3	0.01 (0.02)	1.90 (0.12)	Yb	0.001	0.081	0.001	0.026
Lu_2O_3	0.00 (0)	0.21 (0.03)	Lu	0	0.009	0	0.003
PbO	0.59 (0.14)	0.00 (0)	Pb	0.025	0.000	0.015	0.000
ThO_2	5.56 (0.86)	0.12 (0.07)	Th	0.202	0.004	0.117	0.001
UO_2	0.48 (0.37)	0.01 (0.01)	U	0.017	0.000	0.010	0.000
Total	99.14	96.70	Total	7.995	8.007		

Notes: Monazite: Kakola, Turku, Finland, sample A64a, U–Pb age 1.82 billion years (Suominen, 1991), average of 24 analyses of 12 zoned and unzoned grains. Xenotime: Ibitiara City, Bahia, Brazil, average of 26 analyses of 3 scans across single crystal, Gd concentration corrected for overlap of Gd and Ho L lines.

starting solutions. In these cases, the following approximation was used:

$$C_{\mathrm{NaCl+HCl}} = a_3\Delta^3 + a_2\Delta^2 + a_1\Delta + a_0 \quad (2)$$

where $C_{\mathrm{NaCl+HCl}}$ is the actual total NaCl+HCl concentration of the solution in wt.% relative to H_2O, and Δ the measured freezing point depression of the ternary mixture in °C ($0 \le \Delta < 21$ °C). Ignoring the contribution of ternary interaction to the vapor-saturated ice liquidus surface, the coefficients $a_0..a_3$ for the ternary solution were obtained by linear interpolation of the coefficients for the binary systems H_2O+NaCl and H_2O+HCl using the known initial HCl/NaCl weight ratio of the solution. The coefficients for H_2O+NaCl were taken from Eq. (1) in Bodnar and Vityk (1994): $a_0=0$, $a_1=1.78$, $a_2=-0.0442$, and $a_3=0.000557$. The coefficients for H_2O+HCl were fitted based on data listed by Gmelin (1968) and Wolf et al. (1981): $a_0=0.04$, $a_1=0.9964$, $a_2=-0.03097$, and $a_3=0.00053$. Because X_{HCl} was far below the azeotropic concentration (e.g., Gmelin, 1968) and the partial pressures of HCl and NaCl are much lower than that of water at 20 °C, it was assumed that the HCl/NaCl ratio remained constant during evaporation. This ratio and the determined $C_{\mathrm{NaCl+HCl}}$ were then used to calculate the actual molalities of HCl and NaCl in the solution after loading into the sample chamber of the HDAC. The error associated with this empirical approach should be very small in the case of the H_2O+NaCl+HCl compositions used in our experiments because the solutions contained much more NaCl than HCl.

After sealing and cryometry, the cell was mounted in the position for optical observation on the *xyz*-stage of the SR-XRF spectrometer (Fig. 1b). The cell was then heated and the sample chamber was monitored to check for leaks and to ensure that only a single fluid phase was present in the analytic volume at the experimental temperature (i.e., no gasket creep or crystal movement into the recess in the lower anvil). The HDAC was heated externally by NiCr coils around the tungsten carbide seats, which support the anvils. During heating, the cells were flushed with 400 l/h Ar+1% H_2 or N_2+1% H_2 gas to prevent oxidation of metallic parts in the interior of the HDACs. The temperature was measured using K-type (NiCr/NiAl) thermocouples attached to the diamonds and controlled using Eurotherm® 2408 temperature controllers, which held the set temperature within ±0.5 °C. The actual temperature in the sample chamber was calibrated to ±1.5 °C based on measurement of the melting points at atmospheric pressure of azobenzene

(68 °C), sodium nitrate (306.8 °C), and sodium chloride (800.5 °C). The temperature difference between the recess in the anvil and the location of the REE phosphate crystal was small (< 1 °C at the melting temperature of $NaNO_3$).

When the desired experimental temperature was reached, the time was noted and the cell was rotated around the *z*-axis by 40° into the SR-XRF measurement position (Fig. 1b). The sample chamber was then aligned with the beam and the fluorescence detector. After alignment, consecutive SR-XRF spectra were recorded to determine the concentration of elements in the fluid as a function of time. The cell was then rotated back into the position for optical observation of the sample chamber. Unless the experiment was conducted at vapor pressure, the cell was subsequently cooled, and the liquid–vapor homogenization temperature $T_{h(L+V\rightarrow L)}$ was measured. Successive runs were performed at different, generally higher, experimental *P*–*T* conditions. During first heating, the sample chamber diameter and thus the fluid volume usually decreased due to gasket creep (Schmidt and Rickers, 2003). The run series were stopped when, during heating, gasket material moved into the recess in the anvil at the side directed towards the detector, or when the fluid density was too high for the renucleation of a vapor bubble upon cooling. If no vapor bubble renucleated, the liquidus temperature of the fluid $T_{m(I+L\rightarrow L)}$ (ice melting without the presence of vapor) was measured.

The experiments were conducted at the SR-XRF microprobe at the Hamburger Synchrotronstrahlungslabor HASYLAB at beamline L of DORIS III at Deutsches Elektronen-Synchrotron DESY, Hamburg, Germany. All spectra were recorded using an HPGe energy-dispersive detector aligned at 90° to the beam. The spectra collection real times varied from 100 to 1000 s. For most experiments, the same configuration was used as described by Schmidt and Rickers (2003): a polychromatic beam collimated with a cross-slit system to a size of $50\times50\ \mu m^2$, Al absorbers (thickness 12 mm or 16 mm) for low-energy cut-off to improve peak to background ratios, and HDACs with a recess in the gasket to keep the crystal out of the path of the X-ray beam. The polychromatic beam set-up permitted simultaneous analysis of the REE and other elements ($Z>25$).

Some experiments were performed using a pink multilayer beam with photon energies of 22.3 ± 0.1 keV and a single bounce capillary (SBC) to optimize for the detection of Y, Pb, Th, and U. A 1 mm thick Al absorber was applied to protect the multilayer optics. The single bounce capillary (SBC) was developed and manufactured at Cornell University for the specific requirements of hydrothermal diamond-anvil cell experiments (Falkenberg et al., 2003). It has a focal distance of 5 cm and focuses hard X-rays up to 40 keV into a spot of $11\pm1\ \mu m$ (Fig. 1). A micro-beamstop was aligned at the beam entrance into the SBC to absorb the portion of the beam that would pass the capillary without reflection. Utilization of the SBC increased the flux density by a factor of 300, and the lower limits of detection of elements in the energy range from 12 to 20 keV decreased by one order of magnitude to 1 to 5 ppm in HDAC experiments. Furthermore, the focused beam permitted dispensation of the recess in the gasket in which the mineral grain is placed. This facilitated application of Ir gaskets in high-temperature experiments (Schmidt et al., 2003). Although Re has better mechanical properties than Ir, particularly with respect to its creep behavior, it is much less resistant to aggressive fluids. We observed a significant reaction of the Re gasket with H_2O + HCl at temperatures $\geq$ 600 °C, which was indicated by a rapid decrease in the intensity of the La Kα lines in the XRF spectra of the fluid with time.

All obtained spectra were normalized to 100 mA to account for differences in the DORIS III current and to a live time of 1000 s. If only one element was analyzed (in case of the $LaPO_4$ and xenotime dissolution experiments), the La or Y $K\alpha_1+\alpha_2$ peak areas were obtained using Peakfit v. 4.02 (Jandel Scientific Software) to minimize the error in the area related to peak fitting. The peak areas were then divided by the fluid density at the experimental *P*–*T* conditions (see next paragraph for details of the density determination). The molal concentration at the experimental pressure and temperature was calculated from a calibration curve of the density-corrected peak area per 1000 s collection time vs. the element molality in the fluid. Multi-element XRF spectra with strong peak overlaps obtained in the natural monazite dissolution experiments were processed using the software package AXIL (Van Espen et al., 1986; Vekemans et al., 1995). Correction factors relative to a calibrated reference element (La for the REE and Rb for U, Th, Pb, and Y) were determined using a Monte Carlo simulation code (Vincze et al., 1993, 1995a,b) to avoid empirical calibration for every single element. This code takes into account geometric parameters (e.g., cell geometry, sample-detector alignment), the composition and density of the materials in the path of the X-rays, the fluorescence yield of the elements in the sample and sample-related absorption effects, the excitation spectrum (linear polarisation, absorbers), and the detector efficiency. For the experimental set-up used in our study, the code predicts adequately the intensity ratios of the fluorescence lines of elements if the fluorescence energies are similar. Four different standard solutions were used: a 10,029 mg La/l solution, a La-, Nd- and Gd- solution (333 μg/g each), both in a matrix of H_2O + 5 vol.% HNO_3 (relative to H_2O),

and two aqueous 10 wt.% NaCl solutions with Rb and Cs (250 and 1000 μg/g each). The actual element concentrations in the standard solutions in the cells after loading were obtained from cryometry, i.e., the HNO_3 or NaCl concentration in the sample chamber was determined from the measured freezing point depression and the actual concentration of La or Rb was calculated from the known La/HNO_3 or RbCl/NaCl ratio. In addition, some tests were performed using powders of the standard reference materials NIST610 and NIST612 loaded into the sample chamber of the cells. The standardization spectra were acquired at the same analytical conditions than those of the dissolution experiments. The analytical accuracy of the element concentrations determined in this study depends mainly on the signal to noise ratio of the spectra and should mostly be much better than ±25% (Schmidt and Rickers, 2003) unless the concentrations were close to the lower limit of detection. Quantification of the lead concentration was generally difficult due to overlaps of the Pb L lines with other lines in the SR-XRF spectra resulting in a lower analytical precision for Pb compared to that of all other analyzed elements. For experiments at vapor pressure, some additional uncertainty in the element molalities stems from the possible presence of a vapor fraction in the excitation volume in the anvil recess during spectra recording. The data were discarded if this was indicated from optical monitoring or too low concentrations.

In most cases, the fluid density at the experimental P–T conditions was obtained from the homogenization temperature $T_{h(L+V\rightarrow L)}$ measured after cooling from the experimental temperature, and the cryometrically determined fluid composition. For H_2O+HCl fluids, the density was calculated based on the density of pure water at $T_{h(L+V\rightarrow L)}$ and the density of a fluid with $X_{HCl}=0.11$ at the same $T_{h(L+V\rightarrow L)}$. The density of pure water at vapor saturation was taken from the NBS/NRC Steam Tables (Haar et al., 1984). For the fluid density along the high-pressure portion of the solvus of $X_{HCl}=0.11$, we obtained the following equation based on the data provided by Austin and Glowacki (1989), Hisham and Bommaraju (1995), and Sharygin and Wood (1997):

$$\begin{aligned}\rho_S\ (\text{at } X_{HCl}=0.11) &= -3.61\cdot10^{-13}\cdot T_S^5 \\ &\quad +2.12948\cdot10^{-10}\cdot T_S^4 \\ &\quad -4.61715\cdot10^{-8}\cdot T_S^3 + 3.526\cdot10^{-6}\cdot T_S^2 \\ &\quad -5.5763\cdot10^{-4}\cdot T_S + 1.1074 \end{aligned} \quad (3)$$

where T_S is the solvus temperature ($T_S=T_{h(L+V\rightarrow L)}$) and ρ_S is the fluid density at the solvus. These two densities (of pure water and of $X_{HCl}=0.11$) for a given measured $T_S=T_{h(L+V\rightarrow L)}$ were then used to derive a linear equation from which the density of the H_2O+HCl fluid at the solvus was calculated. This procedure is only valid for $0\le T_S\le 373$ °C and $0\le X_{HCl}<0.12$. Within these ranges, a linear relationship is a good approximation to describe the fluid density as a function of X_{HCl} at constant T_S. This is indicated by the very small deviations (≤ 0.0033 g/cm^3) of densities calculated in this manner from data listed by Austin and Glowacki (1989) for 5 and 10 wt.% HCl ($X_{HCl}=0.0253$ and 0.052), which were not used to derive Eq. (3). If no vapor bubble renucleated upon cooling, the pressure at the liquidus was approximated from the temperature difference of the measured $T_{m(I+L+V\rightarrow L+V)}$ before and $T_{m(I+L\rightarrow L)}$ after the experiment and a reasonable estimate for dT/dP slope of the

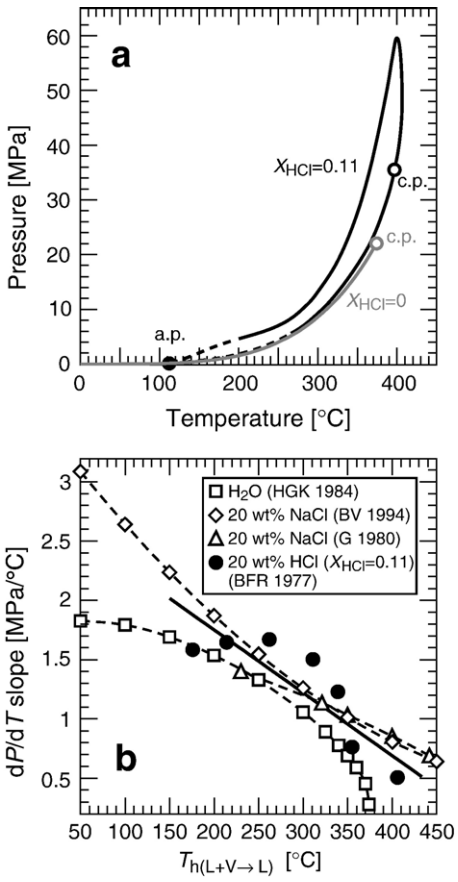


Fig. 2. a) Pressure–temperature diagram showing the liquid–vapor curve of water (grey line, from data in Haar et al., 1984) and the H_2O+HCl solvus of $X_{HCl}=0.11$ (black line) obtained from phase diagrams in Bach et al. (1977) and Hisham and Bommaraju (1995). c.p. — critical point, a.p. — azeotropic point of $X_{HCl}=0.11$. b) Isochore dP/dT slopes of H_2O± HCl±NaCl fluids as a function of the homogenization temperature $T_{h(L+V\rightarrow L)}$. Squares — H_2O (Haar et al., 1984), diamonds — 20 wt.% NaCl, iso-Th-lines (Bodnar and Vityk, 1994), triangles — 20 wt.% NaCl (Gehrig, 1980), circles — 20 wt.% HCl ($X_{HCl}=0.11$), from Fig. 2 in Bach et al. (1977) (solid line — linear fit of these data).

Table 2
Summary of experimental conditions and results of the monazite and xenotime dissolution experiments in H_2O+HCl±NaCl

Experimental conditions	T_E (°C)	P_E (MPa)	$T_{h(L+V\rightarrow L)}$ (°C)	ρ_F (g/cm^3)	*pH*	Element concentration in fluid (mol/kg)
Xenotime Ibitiara City	250	4.5	P_v	0.843	0.19	Y 2.94E-04
1.88 *m* HCl	300	10	P_v	0.756	0.51	Y 5.57E-04
$T_{m(I+L+V\rightarrow L+V)}$=−8.2 °C	350	20	350 (P_v)	0.601	1.00	Y 6.49E-04
Ir gasket, HDAC-2b	450	200	281	0.794	0.83	Y 1.98E-03
Pink beam (22 keV)+SBC	500	290	268	0.816	0.89	Y 2.65E-03
	600	1320	53	1.015	–	Y 4.76E-03
$LaPO_4$ Uba5-VIII	25	0.1	P_v	1.072	−0.50	La 2.84E-02
5.11 *m* HCl	100	0.1	106 (P_v)	1.035	−0.53	La 1.32E-02
$T_{m(I+L+V\rightarrow L+V)}$=−33.0 °C	150	0.5	161 (P_v)	1.002	−0.45	La 2.86E-02
Ir gasket, HDAC-3						
Polychromatic beam						
$LaPO_4$ Uba5-VIII	100	0.1	P_v	1.023	−0.47	La 1.03E-02
4.25 *m* HCl	150	0.5	P_v	0.989	−0.39	La 1.68E-02
$T_{m(I+L+V\rightarrow L+V)}$=−24.8 °C	200	1.8	P_v	0.948	−0.25	La 2.56E-02
Ir gasket, HDAC-3						
Polychromatic beam						
$LaPO_4$ Uba5-VIII	250	60	214	0.909	−0.04	La 1.90E-02
2.93 *m* HCl	300	180	195	0.928	−0.03	La 3.63E-02
$T_{m(I+L+V\rightarrow L+V)}$=−14.6 °C	350	1300	On liquidus, $T_{m(I+L\rightarrow L)}$=−24.8 °C	1.089[a]	–	La ≥5.59E-02
Ir gasket, HDAC-3						
Polychromatic beam						
$LaPO_4$ Uba5-VIII	26	0.1	P_v	1.037	−0.28	La >4.8E-03[b]
2.64 *m* HCl	100	0.1	P_v	1.000	−0.30	La 6.6E-03
$T_{m(I+L+V\rightarrow L+V)}$=−12.7 °C	200	1.7	P_v	0.918	−0.11	La 1.44E-02
Ir gasket, HDAC-3	300	160	202	0.916	0.03	La 3.28E-02
Polychromatic beam	350	560	102	0.998	–	La 4.93E-02
$LaPO_4$ Uba5-VIII	26	0.1	P_v	1.013	0.06	La >3.1E-03[b]
1.02 *m* HCl	98	0.1	P_v	0.976	0.05	La 4.5E-03
$T_{m(I+L+V\rightarrow L+V)}$=−4.0 °C	200	1.6	P_v	0.886	0.18	La 6.2E-03
Re gasket, HDAC-2	300	70	248	0.826	0.46	La 1.08E-02
Polychromatic beam	450	300	235	0.844	0.73	La 2.11E-02
	600	480	244	0.832	1.15	La ≈3.2E-02
$LaPO_4$ Uba5-VIII	200	90	159	1.067	1.05	La 2.4E-03
0.24 *m* HCl, 4.73 *m* NaCl	300	1060	<30 (≈ 0)	1.282	–	La 3.3E-03
$T_{m(I+L+V\rightarrow L+V)}$=−20.2 °C						
Ir gasket, HDAC-2						
Polychromatic beam						
$LaPO_4$ Uba5-VIII	700	570	282	0.933	–	La b.d.l. (<6E-04)
1.99E-05 *m* HCl, 3.98 *m* NaCl						
$T_{m(I+L+V\rightarrow L+V)}$=−15.3 °C	800	1050	211	0.994	–	La ≈ 6E-04?[c]
Ir gasket, HDAC-2						
Polychromatic beam						

(continued on next page)

Table 2 (*continued*)

Experimental conditions	T_E (°C)	P_E (MPa)	$T_{h(L+V\rightarrow L)}$ (°C)	ρ_F (g/cm^3)	*pH*	Element concentration in fluid (mol/kg)
Monazite Kakola 6.09 *m* HCl $T_{m(I+L+V\rightarrow L+V)}$=−44.0 °C Ir gasket, HDAC-3b Polychromatic beam	100	0.1	P_v	1.048	−0.58	La 1.25E-02 (Peakfit) La 1.26E-02 (AXIL) Ce 2.67E-02 Pr 3.3E-03 Nd 1.10E-02 Sm 1.6E-03 Gd 7E-04 Y 4E-04 Pb b.d.l. Th 8E-04 U b.d.l.
	150	0.5	166(P_v)	1.017	−0.50	La 1.28 E-02 (Peakfit) La 1.32 E-02 (AXIL) Ce 2.75E-02 Pr 3.6E-03 Nd 1.10E-02 Sm 1.6E-03 Gd 7E-04 Y 4E-04 Pb b.d.l. Th 9E-04 U b.d.l.
	200	110	151	1.016	−0.50	La 2.20E-02 (Peakfit) La 2.17E-02 (AXIL) Ce 4.62E-02 Pr 6.1E-03 Nd 2.00E-02 Sm 3.0E-03 Gd 1.3E-03 Y 6E-04 Pb 7E-04 Th 1.7E-03 U 2E-04
Monazite Kakola	25	0.1	P_v	1.063	−0.45	–[d]
4.42 *m* HCl	100	0.1	P_v	1.025	−0.48	–[d]
$T_{m(I+L+V\rightarrow L+V)}$=−26.3 °C	150	0.5	P_v	0.991	−0.40	–[d]
Ir gasket, HDAC-3c Pink beam (22 keV) +SBC						
Monazite Kakola	300	150	207	0.893	0.15	–[d]
1.76 *m* HCl	450	1200	<65 (≈ 0)	1.03	–	–[d]
$T_{m(I+L+V\rightarrow L+V)}$=−7.6 °C	600	1980	On liquidus, $T_{m(I+L\rightarrow L)}$=−31.6 °C	1.096	–	–[d]
Ir gasket, HDAC-2 Pink beam (22 keV) +SBC						

The listed element concentrations in the fluid represent averages of in situ SR-XRF analyses that showed no significant change in the normalized peak areas in consecutive spectra.

T_E=experimental temperature; P_E=experimental pressure, calculated from $T_{h(L+V\rightarrow L)}$ using the equation of state of H_2O+NaCl of Bodnar and Vityk (1994) and assuming wt.% (HCl+NaCl)=wt.% NaCl (weight percent relative to H_2O); $T_{h(L+V\rightarrow L)}$=liquid–vapor homogenization temperature, homogenization to the liquid phase; ρ_F=calculated fluid density; *pH*=calculated *pH* at T_E and P_E based on the dissociation constants of HCl° to 700 °C and 500 MPa from Tagirov et al. (1997); P_v=experiment at vapor pressure; $T_{m(I+L+V\rightarrow L+V)}$=ice melting temperature in the presence of vapor; $T_{m(I+L\rightarrow L)}$=liquidus temperature (ice melting without vapor presence), SBC=single bounce capillary; [a] liquidus pressure approximated based on liquidus slope for 9.66 wt.% NaCl (Bodnar, 1994) and density calculated from data provided by Sobol' et al. (1991) and Sharygin and Wood (1997); [b] concentration too low (vapor bubble in excitation volume or time insufficient for equilibration); [c] *m* La in fluid was below or close to detection limit; [d] not calibrated, only element ratios determined; b.d.l.=below detection limit.

liquidus based on liquidi slopes in the system H_2O+NaCl (Bodnar, 1994) and the ice I melting curve (Wagner et al., 1994). The density was then calculated based on compressibility data for hydrochloric acid at 25 °C (Sobol' et al., 1991; Sharygin and Wood, 1997). For H_2O+NaCl+HCl solutions, the density at the solvus was calculated from the determined homogenization temperature $T_{h(L+V\rightarrow L)}$ and the salinity $C_{NaCl+HCl}$ from Eq. (2) using the program MacFlinCor (Brown and Hagemann, 1994) and H_2O+NaCl as model system.

An equation of state for H_2O+HCl fluids applicable at all P–T–X conditions of our experiments was not available. Therefore, the pressure P_E at the experimental temperature was calculated based on the following approach:

$$P_E = P_S + (dP/dT)\cdot(T_E - T_{h(L+V\rightarrow L)}) \quad (4)$$

where P_S is the pressure at the solvus, dP/dT the isochore slope, and T_E the experimental temperature. For densities above that at the vapor-saturated liquidus, P_S was substituted by the pressure at the liquidus and $T_{h(L+V\rightarrow L)}$ by the measured liquidus temperature $T_{m(I+L\rightarrow L)}$. The solvus pressure was obtained by linear interpolation between the pressure of the liquid–vapor curve of pure water at $T_{h(L+V\rightarrow L)}$ (Haar et al., 1984) and the pressure of the high-density portion of the H_2O+HCl solvus of X_{HCl}=0.11 at the same $T_{h(L+V\rightarrow L)}$. The P–T location of the solvus of X_{HCl}=0.11 was obtained from phase diagrams provided by Bach et al. (1977) and Hisham and Bommaraju (1995) (Fig. 2a). The dependence of the solvus pressure on composition is approximately linear in the compositional range $0 \le X_{HCl} \le 0.11$ (Bach et al., 1977). The isochore slopes of the H_2O+HCl±NaCl fluids were approximated using those in the system H_2O+NaCl (Bodnar and Vityk, 1994) at the same $T_{h(L+V\rightarrow L)}$ and assuming wt.% (HCl+NaCl)=wt.% NaCl for the input NaCl concentration. At $T_{h(L+V\rightarrow L)}$ between 175 °C and 405 °C, the validity of this assumption is supported by the relatively good agreement between the linear fit of the isochore slopes for X_{HCl}=0.11 (=20 wt.% HCl) taken from Fig. 2 in Bach et al. (1977) and the slopes of H_2O+20 wt.% NaCl isochores (Gehrig, 1980) and iso-T_h-lines (Bodnar and Vityk, 1994) (Fig. 2b). No data were available at X_{HCl}=0.11 and $T_{h(L+V\rightarrow L)}$<175 °C or at lower HCl concentrations. The isochore slopes from Fig. 2 in Bach et al. (1977) were obtained over a small pressure interval (<150 MPa), which would result in a large additional uncertainty upon extrapolation of the isochores to higher pressures. Furthermore, these data show an unrealistic trend at $T_{h(L+V\rightarrow L)}$<260 °C, i.e. decreasing dP/dT slopes with decreasing $T_{h(L+V\rightarrow L)}$ (Fig. 2b). For these reasons, iso-T_h-line slopes of H_2O+NaCl fluids (Bodnar and Vityk, 1994) were used to approximate P_E in our study. It should further be noted that the equations provided by Bodnar and Vityk (1994) for the dP/dT slope of H_2O+NaCl iso-T_h-lines are based on experimental data to pressures of 600 MPa and $T_{h(L+V\rightarrow L)} \ge 50$ °C. For some of our experiments, extrapolation beyond these conditions was required to calculate P_E. Pressures above 600 MPa listed in Table 2 are probably overestimated (cf., Fig. 2b). Overall, the insufficiently known P–T trajectories of the isochores in the system H_2O+HCl are the largest source of error in the pressures calculated from Eq. (4).

The pH at T_E and P_E was calculated by solving Eq. (5) for m_{H+}:

$$K_{D(HCl°)} = m_{H+}(m_{H+} + m_{NaCl})/(m_{HCl} - m_{H+}) \quad (5)$$

where $K_{D(HCl°)}$ are the dissociation constants of HCl° to 700 °C and 500 MPa from Tagirov et al. (1997) and m_{NaCl} and m_{HCl} are the determined actual molalities of NaCl and HCl in the solution after loading.

3. Results, discussion, and conclusions

The conditions and some results of the monazite and xenotime leaching experiments are summarized in Table 2. We do not report solubility products because it was not possible to measure the P concentration in the fluid in situ using SR-XRF analyses and because even end-member REE phosphates tend to dissolve incongruently (Poitrasson et al., 2004; Cetiner et al., 2005). The lack of appropriate experimental techniques to analyze P and other light elements at lower concentrations in fluids is presently the main obstacle for in situ mineral solubility studies at high pressures and temperatures. The intensity of the PO_4 stretching modes in Raman spectra can potentially be used for the in situ analysis of phosphorus at relatively high concentrations but has not been calibrated yet. Thus, we focused in this study on the release kinetics and the relative mobility of the heavy elements Y, the REE, Pb, Th, and U.

3.1. Dissolution kinetics and attainment of equilibrium

In all experiments reported in Table 2, equilibrium was approached from undersaturation. Reversal of the experiments, i.e. to attain equilibrium from supersaturation, is problematic, as demonstrated by a second heating run in the leaching experiments of xenotime in 1.9 *m* HCl. The

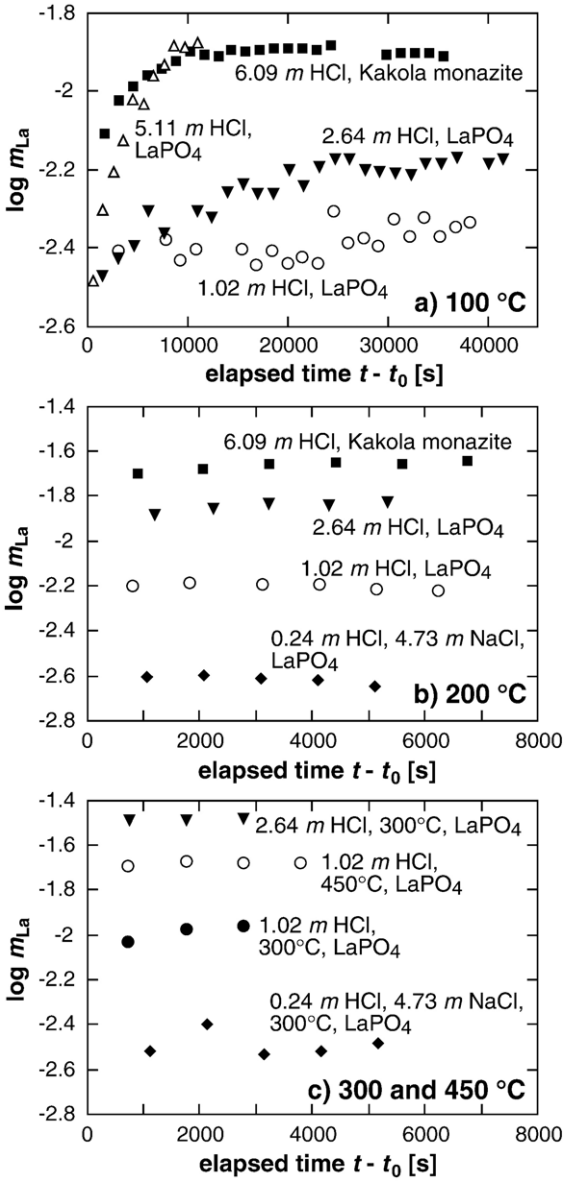


Fig. 3. Temporal evolution of the logarithm of La molality in the fluid during dissolution of synthetic $LaPO_4$ monazite and monazite from Kakola, Finland, at 100 °C (a), 200 °C (b), and 300 and 450 °C (c) in 6.09 *m* HCl (squares), 5.11 *m* HCl (open triangles), 2.64 *m* HCl (filled triangles), 1.02 *m* HCl (circles), and 0.24 *m* HCl+4.73 *m* NaCl (diamonds). t_0 is the time at which the experimental temperature was attained. For consistency, all La concentrations in the fluid including those during leaching of Kakola monazite are based on the La $K\alpha_1+\alpha_2$ peak areas obtained using Peakfit v. 4.02.

results of the first run are listed in Table 2. After subsequent cooling from 600 °C to 25 °C and reheating, the measured Y concentration at 350 °C was significantly higher than any obtained in the first run. This was probably due to microscopically invisible precipitates, which were still present in the anvil recess. Upon further heating, the Y concentration first decreased and became then constant between 450 and 600 °C at a value close to that obtained during the first run at 600 °C. These results suggest that equilibrium was reached in the first series at least at 600 °C.

Fig. 3 shows the La molality in the fluid during dissolution of synthetic $LaPO_4$ and natural monazite as a function of time for temperatures from 100 to 450 °C and various HCl±NaCl concentrations. At temperatures ≥ 300 °C, constant (within error) La concentrations were attained rapidly in less than 50 min (Fig. 3c). At 200 °C, the aqueous La concentration became constant in less than 1.5 h (Fig. 3b). More sluggish dissolution kinetics and a dependence on the HCl molality were observed in the experiments at 100 °C. At the highest HCl concentrations (6.1 and 5.1 *m* HCl), apparent equilibrium was reached after about 2.5 to 3 h, whereas 7 h were required to attain a constant La molality at 2.6 *m* HCl. At 1 *m* HCl, the dissolution kinetics was probably even more sluggish (Fig. 3a) but difficult to evaluate because the La concentrations were close to the lower limit of detection (log $m_{La}=-3.22$), which resulted in a large scatter in the data. In that run, it is possible that equilibrium was not attained even after 11 h. The temperature dependence of the dissolution kinetics in our experiments is in good agreement with the observations of Cetiner et al. (2005) although particle size and solid/solution ratio were about one order of magnitude lower in their experiments. In their study, constant concentrations of La, Sm, and Nd were attained in H_2O+HCl+NaCl solutions ($pH=1.0$ to 1.3) in less than 2 to 3 days at 50 °C and 15 to 20 days at 23 °C,

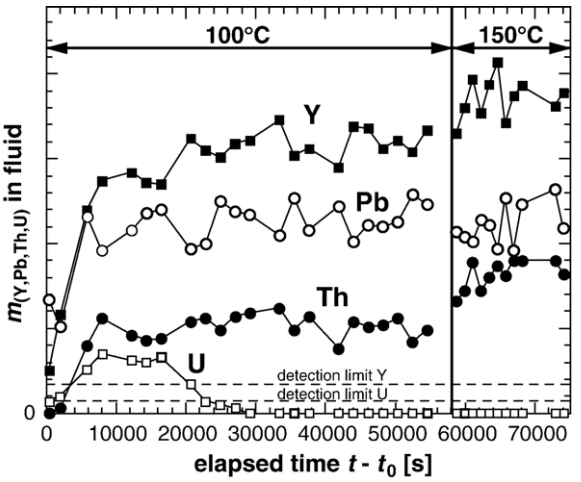


Fig. 4. Diagram of the relative molalities of Y, Pb, Th, and U in the fluid vs. time during leaching of monazite from Kakola, Finland, in 4.42 *m* HCl at vapor pressure. Note that no absolute concentrations are given because of an invalid calibration.

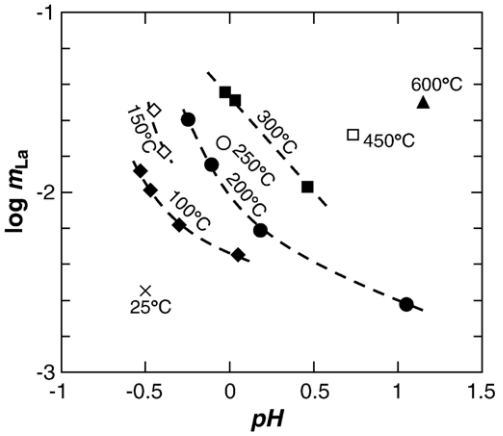


Fig. 5. Plot of the logarithm of the La molality in the fluid vs. calculated *pH*.

whereas Y displayed much slower kinetics. Poitrasson et al. (2004) found that the Nd, Gd, and P concentrations were constant in less than 2 months in monazite end-member solubility experiments at $pH=2$ and 21 and 70 °C but the Nd concentration continued to increase at 200 and 300 °C, coupled with a decrease in the P concentration. We do not know if such a variation in the REE and Y concentrations would also occur at temperatures ≥200 °C in our experiments, in which the solid/solution ratios and HCl concentrations are much higher. We did not conduct long-term HDAC runs at high temperatures because their feasibility is unknown. Impurities in the starting materials, such as phosphates that are more soluble than the REE phosphate, can also affect the REE concentrations in the fluid (Poitrasson et al., 2004; Cetiner et al., 2005). In our experiments, contamination had probably little effect on the data, although small amounts of excess $La(OH)_3$ were present in the synthetic $LaPO_4$ charge (U. Anderson, personal communication). This is because we used cleaned and hand-picked single crystals and because of the high REE concentrations in the fluid in this study, which minimize the possible effect of a $La(OH)_3$ contamination in the ppm range. The element molalities in the fluid given in Table 2 represent averages of data from SR-XRF spectra in which the normalized peak areas remained, within error, constant with respect to time. We interpret these data tentatively as equilibrium or near equilibrium concentrations for temperatures ≥200 °C. For a discussion of the relative element mobility, it is less important whether they are actually steady state concentrations.

The release behavior of Ce, Pr, Nd, Sm, Gd, Y, and Th was very similar to that of La in the Kakola monazite leaching experiments in 6.1 *m* HCl shown in Fig. 3. The release kinetics were perhaps somewhat more sluggish in the case of Y at 100 °C. Uranium and Pb were only detectable in the experiment at 200 °C and the precision of these data did not permit to evaluate the time dependence. Thus, the SBC was used in a leaching run of Kakola monazite in 4.4 *m* HCl to optimize the analytic conditions for Y, Pb, Th, and U. In this experiment, the U XRF lines disappeared from the spectra of the fluid after 6 h at 100 °C and the U concentration remained below the detection limit after heating to 150 °C (Fig. 4). This indicates that U was reincorporated into monazite or precipitated in a second solid phase. At 100 °C, Th and Pb displayed constant concentrations with respect to time after about 2 to 2.5 h, whereas the data again suggest a slower release of Y into the fluid.

3.2. La complexation in the experimental solutions

Fig. 5 shows that the determined La concentration in $H_2O+HCl\pm NaCl$ fluids decreases with increasing *pH* along all isotherms between 100 and 300 °C. Although our solutions were very acidic, this negative slope indicates that positively charged La complexes control the solubility at these conditions. This is in agreement with previous studies on Nd (Migdisov and Williams-Jones, 2002; Poitrasson et al., 2004). The most abundant complexes are probably $LaCl^{2+}$ and $LaCl_2^+$ (Haas et al., 1995; Gammons et al., 1996; Migdisov and Williams-

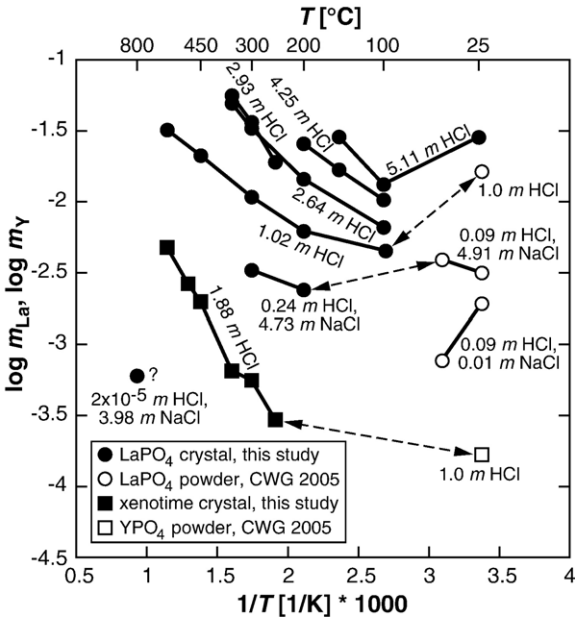


Fig. 6. Comparison of experimental data for Y (squares) and La (circles) concentrations in $H_2O+HCl\pm NaCl$ fluids in or near equilibrium with xenotime or $LaPO_4$ monazite as a function of temperature. Filled symbols — this study, open symbols — data from Cetiner et al. (2005) (CWG 2005). The arrows connect data from both studies at the same or approximately similar fluid compositions.

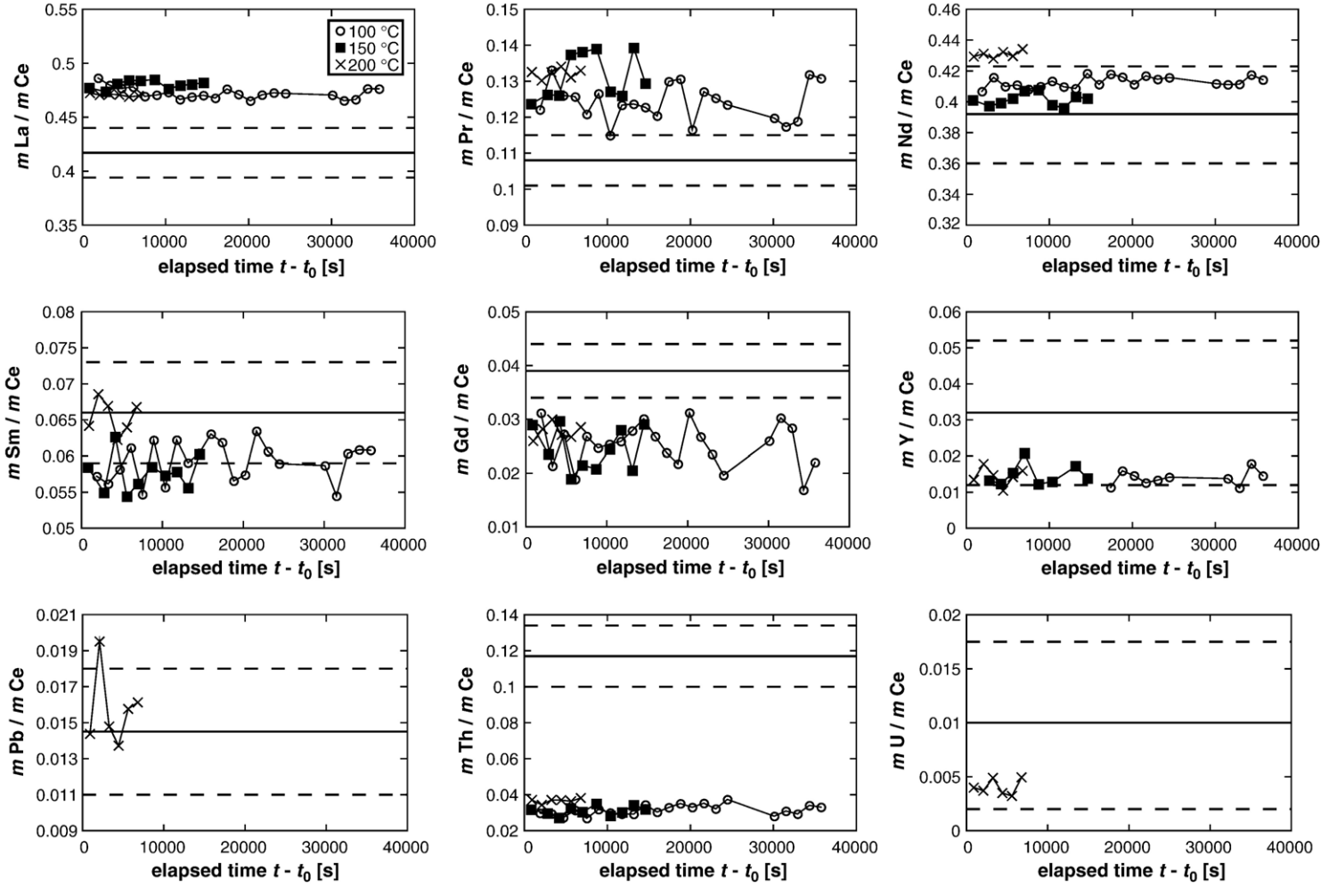


Fig. 7. Aqueous metal concentration ratios relative to Ce during dissolution of natural monazite (Kakola, Turku, Finland) in 6.09 *m* HCl at 100 °C (circles), 150 °C (squares), and 200 °C (crosses). Y/Ce ratios were omitted if the signal to noise ratio in the spectra did not permit a reliable fit of the Y Kα peak area. The U/Ce and Pb/Ce ratios are not shown for the experiments at 100 and 150 °C because the concentrations of U and Pb were close or below the detection limit in most spectra. Dashed lines indicate $\pm 1\sigma$ from the average monazite composition (thick solid line). The same monazite grains were used for all experiments.

Jones, 2002). The trend of our data suggests that there is no qualitative change in the La speciation at temperatures above 300 °C (Fig. 5), i.e., the predominance of positively charged La complexes continues.

3.3. Rare-earth element and yttrium mobility

Experimental data for Y and La concentrations in H_2O+HCl±NaCl fluids in or near equilibrium with xenotime or $LaPO_4$ monazite obtained by Cetiner et al. (2005) and in this study are shown as a function of temperature in Fig. 6. Above 100 °C, the La and Y concentrations always increased with temperature, which suggests prograde REE phosphate solubility. However, linear extrapolation of our high-temperature in situ data for the La and Y molality in the fluid to 23 and 50 °C results in concentrations which are about one order of magnitude lower than determined by Cetiner et al. (2005) at the same or roughly similar fluid compositions (arrows in Fig. 6). This large discrepancy can not be attributed to a significant $La(OH)_3$ contamination in our experiments, which should rather increase the La molality in the fluid. The simplest explanation is that equilibrium was not attained in our experiments, which cannot be ruled out, particularly in case of Y at lower temperatures. However, this should not cause a large discrepancy in the La molalities because the results for the dissolution kinetics from both studies are consistent. Another reason could be the existence of a solubility minimum. $LaPO_4$ and $NdPO_4$ were found to display retrograde solubility at zero ionic strength from 23 °C to 70 °C (Firsching and Brune, 1991; Cetiner et al., 2005) and 23 °C to 300 °C (Poitrasson et al., 2004; Cetiner et al., 2005) and the data and calculations in these studies show that retrograde solubility can also be present at acidic conditions. Furthermore, it is conceivable that the larger grain size of the phosphate crystals used in our study resulted in lower solubilities compared to that of the powders used by Cetiner et al. (2005).

Nevertheless, our in situ data show that the Y concentration in the fluid was at least one order of magnitude lower than the La concentration even at the highest *P–T* conditions at which the equilibration should have proceeded very fast (Fig. 6). If the xenotime composition (77 mol% YPO_4 component, see Table. 1) is taken into account, the Y molality in the fluid would only be about a tenth of a log unit higher for pure YPO_4 xenotime assuming an equal Y/HREE ratio in the fluid and the solid. Although H_2O+HCl is not a realistic model system for most natural fluids, acidic and chloridic solutions such as H_2O+$CaCl_2$ are common in the crust. Thus, our experiments indicate a significantly lower mobility of Y compared to that La over a large range of crustal *P–T* conditions if REE phosphates interact with acidic and chloridic fluids. This agrees with observations on natural monazites, which underwent hydrothermal alteration at acidic conditions. Poitrasson et al. (1996) reported that greisenization resulted in a strong decrease of the LREE content of a monazite from the Skiddaw granite, NW England, whereas particularly the Y and also the Er and Yb concentrations increased. Higher Y/La ratios relative to unaltered monazite were found in altered monazites from the St. Nectaire granite, French Massif Central, and from the Carnmenellis granite, SW England, in which sericitization occurred at about 300 to 340 °C and a *pH* of around 4 (Poitrasson et al., 2000). Furthermore, Broska et al. (2005) showed that xenotime was more resistant to low-temperature hydrothermal alteration than monazite, but both minerals were unstable during prograde metamorphism of granitic rocks from the Western Carpathians, Slovakia.

Differences in the mobility of the LREE and HREE+Y are also indicated by the results of the leaching experiments of natural monazite from Kakola, Finland, in 6.1 *m* HCl at temperatures between 100 and 200 °C. The aqueous metal concentration ratios relative to Ce during these experiments are compared with the average metal/Ce ratios in the untreated monazite in Fig. 7. None of the aqueous metal/Ce ratios displayed an obvious temporal evolution (Fig. 7). The scatter in these ratios is mainly related to the statistical error of the measurements. The Nd/Ce, Sm/Ce, and Th/Ce ratios and, less significantly, the Pr/Ce ratio in the fluid increased with temperature.

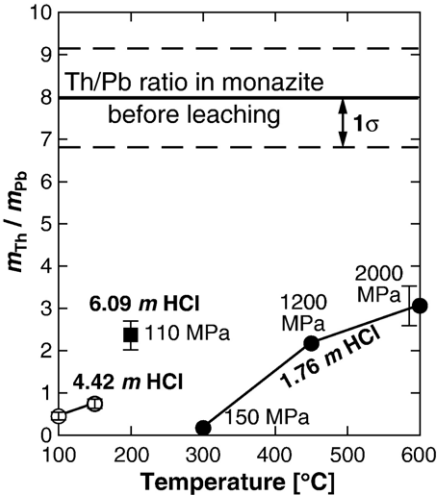


Fig. 8. Th/Pb ratios in the fluid during dissolution of natural monazite (Kakola, Turku, Finland) as a function of temperature for 3 different HCl molalities.

Particularly La and Pr, but also Nd at 200 °C, partitioned more strongly into the fluid than Ce because the metal/Ce ratios in the fluid were higher than those in the untreated monazite. The Gd/Ce, Y/Ce, and, except at 200 °C, the Sm/Ce ratio showed the opposite behavior. These data imply that incongruent dissolution of monazite in H_2O+HCl causes significant changes in the slopes of the REE patterns of fluid and monazite, because the LREE (particularly La) partition more strongly into the fluid than the HREE+Y. This agrees with the conclusion of a higher La mobility relative to Y in the previous paragraph derived from the experiments on xenotime and synthetic $LaPO_4$. Furthermore, the observed La/Ce, Pr/Ce, and Nd/Ce ratios in the fluid during leaching of Kakola monazite in 6.1 *m* HCl solutions are consistent with the closed system experiment at 70 °C and $pH \approx 2$ reported by Oelkers and Poitrasson (2002) if the effect of temperature is taken into account. There is less consistency in the Sm/Ce ratios from both studies.

3.4. Behavior of lead and thorium

The fluid–solid partitioning was insignificant for the Pb/Ce ratio in our leaching experiment in 6.1 *m* HCl. In contrast, the Th/Ce ratio in the fluid, which was 3 to 4 times lower than that in monazite, displayed the most pronounced deviation of any aqueous metal/Ce ratio from the untreated monazite composition (Fig. 7). In closed system experiments at 70 °C, Oelkers and Poitrasson (2002) found a much lower Th/Ce ratio in the fluid relative to that in monazite at *pH* 2, but very similar Th/Ce ratios in fluid and monazite at *pH* 6 and 10. Fig. 8 shows all Th/Pb ratios in the fluid obtained in our study during dissolution of natural monazite from Kakola, Finland in H_2O+HCl. This ratio increased with temperature and HCl concentration in the solution, but was much lower in all experiments than the Th/Pb ratio in the untreated monazite, even at 600 °C and 2 GPa. Seydoux-Guillaume et al. (2002) observed that Pb loss from monazite into the fluid was dependent on fluid composition and temperature. Leaching of monazite in H_2O+$CaCl_2$ at 1000 °C resulted in the formation of a Th-rich and Pb-free rim which did not occur if the solvent was H_2O or if the temperature was 800 °C. All these experiments indicate that hydrothermal alteration in acidic chloridic fluids causes a large increase in the Th concentration relative to that of the LREE and Pb in the reacted monazite.

A very similar style of monazite alteration was observed in nature. A strongly increased Th content and higher Th/Ce and Th/Pb ratios were found in altered monazite from granite, which experienced greisenization (Poitrasson et al., 1996). However, sericitization resulted in generally lower Th/Ce and Th/Pb ratios in the altered monazites because Th was removed and reprecipitated nearby as a separate phase (Poitrasson et al., 2000). The generally limited transport of Th^{4+} by natural aqueous fluids is reflected in the characteristic low ThO_2 contents (mostly less than 0.1 wt.%) in monazites of hydrothermal origin (Schandl and Gorton, 2004).

Acknowledgements

The authors would like to thank Ulf Anderson, Oona Appelt, Bill Bassett, Gerald Falkenberg, Wilhelm Heinrich, Hannu Huhma, Helga Kemnitz, Peter Möller, Franck Poitrasson, Dieter Rhede, Rolf Romer, Georg Schettler, Reiner Schulz, Anne-Magali Seydoux-Guillaume, Rainer Thomas, and Edmund Welter for the samples, microprobe analyses, discussions, support, and assistance with various aspects of this study, the staff of the high-pressure workshop at the GFZ Potsdam for the construction of the high-pressure cells, and HASYLAB at the Deutsches Elektronen-Synchrotron DESY for granting beamtime. Reviews by John Ayers and Joseph Pyle and a review by Franck Poitrasson of an earlier version of the manuscript are greatly appreciated.

References

Andrehs, G., Heinrich, W., 1998. Experimental determination of REE distributions between monazite and xenotime: potential for temperature-calibrated geochronology. Chemical Geology 149, 83–96.

Austin, S., Glowacki, A., 1989. Hydrochloric acid. In: Elvers, B. (Ed.), 5th edition. Ullmann's Encyclopedia of Industrial Chemistry, vol. A13. VCH Verlagsgesellschaft, pp. 283–296.

Ayers, J.C., Watson, E.B., 1991. Solubility of apatite, monazite, zircon, and rutile in supercritical aqueous fluids with implications for subduction zone geochemistry. Philosophical Transactions of the Royal Society of London. A 335, 365–375.

Ayers, J.C., Loflin, M., Miller, C.F., Barton, M.D., Coath, C., 2004. Dating fluid infiltration using monazite. In: Wanty, R.B., SealII II, R.R. (Eds.), Proceedings of the Eleventh International Symposium on Water–Rock Interaction, vol. 1. A.A. Balkema Publishers, pp. 247–251.

Bach, R.W., Friedrichs, H.A., Rau, H., 1977. *p–V–T* relations for HCl–H_2O mixtures up to 500 °C and 1500 bars. High Temperatures – High Pressures 9, 305–312.

Bassett, W.A., Shen, A.H., Bucknum, M., Chou, I.-M., 1993. A new diamond anvil cell for hydrothermal studies to 2.5 GPa and from − 190 to 1200 °C. Reviews of Scientific Instruments 64, 2340–2345.

Bassett, W.A., Anderson, A.J., Mayanovic, R.A., Chou, I.-M., 2000. Modified hydrothermal diamond anvil cells for XAFS analyses of elements with low energy absorption edges in aqueous solutions at sub- and supercritical conditions. Zeitschrift für Kristallographie 215, 711–717.

Boatner, L.A., 2002. Synthesis, structure and properties of monazite, pretulite, and xenotime. Reviews in Mineralogy and Geochemistry 48, 87–121.

Bodnar, R.J., 1994. Synthetic fluid inclusions: XII. The system H_2O–NaCl. Experimental determination of the halite liquidus and

isochores for a 40 wt.% NaCl solution. Geochimica et Cosmochimica Acta 58, 1053–1063.

Bodnar, R.J., Vityk, M.O., 1994. Interpretation of microthermometric data for H_2O–NaCl fluid inclusions. In: De Vivo, B., Frezzotti, M.L. (Eds.), Fluid Inclusions in Minerals, Methods and Applications. Virginia Tech, pp. 117–130.

Braun, I., Montel, J.-M., Nicollet, C., 1998. Electron microprobe dating of monazites from high-grade gneisses and pegmatites of the Kerala Khondalite Belt, southern India. Chemical Geology 146, 65–85.

Broska, I., Williams, C.T., Janák, M., Nagy, G., 2005. Alteration and breakdown of xenotime-(Y) and monazite-(Ce) in granitic rocks of the Western Carpathians, Slovakia. Lithos 82, 71–83.

Brown, P.E., Hagemann, S.G., 1994. MacFlinCor: A computer program for fluid inclusion data reduction and manipulation. In: De Vivo, B., Frezzotti, M.L. (Eds.), Fluid Inclusions in Minerals, Methods and Applications. Virginia Tech, pp. 231–250.

Cesbron, F., 1989. Mineralogy of the rare-earth elements. In: Möller, P., Cerny, P., Saupe, F. (Eds.), Lanthanides, Tantalum and Niobium. Mineralogy, Geochemistry, Characteristics of Primary Ore Deposits, Prospecting, Processing, and Applications. Springer-Verlag, pp. 3–26.

Cetiner, Z.S., Wood, S.A., Gammons, C.H., 2005. The aqueous geochemistry of the rare earth elements. Part XIV. The solubility of rare earth element phosphates from 23 to 150 °C. Chemical Geology 217, 147–169.

Cherniak, D.J., Watson, E.B., Grove, M., Harrison, T.M., 2004. Pb diffusion in monazite: a combined RBS/SIMS study. Geochimica et Cosmochimica Acta 68, 829–840.

Devidal, J.L., Gibert, F., Kieffer, B., Pin, C., Montel, J.-M., 1998. A new method for solubility measurement: application to $NdPO_4$ system in H_2O–NaCl–HCl hydrothermal fluids. Mineralogical Magazine 62A, 375–376.

Evans, J.A., Zalasiewicz, J.A., Fletcher, I., Rasmussen, B., Pearce, N.J.G., 2002. Dating diagenetic monazite in mudrocks: constraining the oil window? Journal of the Geological Society 159, 619–622.

Ewing, R.C., 2001. The design and evaluation of nuclear-waste forms: clues from mineralogy. The Canadian Mineralogist 39, 697–715.

Falkenberg, G., Rickers, K., Bilderback, D.H., Huang, R., 2003. A single-bounce capillary for focusing of hard X-rays. HASYLAB Annual Report 2003, pp. 71–74.

Firsching, F.H., Brune, S.N., 1991. Solubility products of the trivalent rare-earth phosphates. Journal of Chemical and Engineering Data 36, 93–95.

Gammons, C.H., Wood, S.A., Williams-Jones, A.E., 1996. The aqueous geochemistry of the rare earth elements and yttrium: VI. Stability of neodymium chloride complexes from 25 to 300 °C. Geochimica et Cosmochimica Acta 60, 4615–4630.

Gehrig, M., 1980. Phasengleichgewichte und pVT-Daten ternärer Mischungen aus Wasser, Kohlendioxid und Natriumchlorid bis 3 kbar und 550 °C. Doctoral dissertation, Universität Karlsruhe.

Gieré, R., 1996. Formation of rare earth minerals in hydrothermal systems. In: Jones, A.P., Wall, F., Williams, C.T. (Eds.), Rare Earth Minerals. Chapman and Hall, pp. 105–150.

Gmelin, L., 1968. Gmelins Handbuch der Anorganischen Chemie. Chlor. Ergänzungsband, Teil B - Lieferung, vol. 1. Verlag Chemie, Weinheim.

Gratz, R., Heinrich, W., 1997. Monazite–xenotime thermobarometry: experimental calibration of the miscibility gap in the binary system $CePO_4$–YPO_4. American Mineralogist 82, 772–780.

Haar, L., Gallagher, J.S., Kell, G.S., 1984. NBS/NRC Steam Tables: Thermodynamic and Transport Properties and Computer Programs for Vapor and Liquid States of Water in SI Units. Hemisphere Publishing Corporation. 320 pp.

Haas, J.R., Shock, E.L., Sasani, D.C., 1995. Rare earth elements in hydrothermal systems: estimates of standard partial molal thermodynamic properties of aqueous complexes of the rare earth elements at high pressures and temperatures. Geochimica et Cosmochimica Acta 59, 4329–4350.

Harrison, T.M., Catlos, E.J., Montel, J.-M., 2002. U–Th–Pb dating of phosphate minerals. Reviews in Mineralogy and Geochemistry 48, 523–558.

Hisham, M.W.M., Bommaraju, T.V., 1995. Hydrogen chloride, 4th edition. Kirk-Othmer Encyclopedia of Chemical Technology, vol. 13. Wiley, pp. 894–925.

Liu, X., Byrne, R.H., 1997. Rare earth and yttrium phosphate solubilities in aqueous solution. Geochimica et Cosmochimica Acta 61, 1625–1633.

Manning, C.E., Boettcher, S.L., 1994. Rapid-quench hydrothermal experiments at mantle pressures and temperatures. American Mineralogist 79, 1153–1158.

Migdisov, A.A., Williams-Jones, A.E., 2002. A spectrophotometric study of neodymium(III) complexation in chloride solutions. Geochimica et Cosmochimica Acta 66, 4311–4323.

Möller, P., 1989. Rare earth mineral deposits and their industrial importance. In: Möller, P., Cerny, P., Saupe, F. (Eds.), Lanthanides, Tantalum and Niobium. Mineralogy, Geochemistry, Characteristics of Primary Ore Deposits, Prospecting, Processing, and Applications. Springer-Verlag, pp. 171–188.

Oelkers, E.H., Poitrasson, F., 2002. An experimental study of the dissolution stoichiometry and rates of a natural monazite as a function of temperature from 50 to 230 °C and pH from 1.5 to 10. Chemical Geology 191, 73–87.

Philippot, P., Selverstone, J., 1991. Trace-element-rich brines in eclogitic veins: implications for fluid composition and transport during subduction. Contributions to Mineralogy and Petrology 106, 417–430.

Poitrasson, F., Chenery, S., Bland, D.J., 1996. Contrasted monazite hydrothermal alteration mechanisms and their geochemical implications. Earth and Planetary Science Letters 145, 79–96.

Poitrasson, F., Chenery, S., Shepherd, T.J., 2000. Electron microprobe and LA-ICP-MS study of monazite hydrothermal alteration: implications for U–Th–Pb geochronology and nuclear ceramics. Geochimica et Cosmochimica Acta 64, 3283–3297.

Poitrasson, F., Oelkers, E., Schott, J., Montel, J.-M., 2004. Experimental determination of synthetic $NdPO_4$ monazite end-member solubility in water from 21 °C to 300 °C: implications for rare earth element mobility in crustal fluids. Geochimica et Cosmochimica Acta 68, 2207–2221.

Pyle, J.M., Spear, F.S., Rudnick, R.L., McDonough, W.F., 2001. Monazite–xenotime–garnet equilibrium in metapelites and a new monazite–garnet thermometer. Journal of Petrology 42, 2083–2107.

Read, D., Cooper, D.C., McArthur, J.M., 1987. The composition and distribution of nodular monazite in the lower Paleozoic rocks of Great Britain. Mineralogical Magazine 51, 271–280.

Schandl, E.S., Gorton, M.P., 2004. A textural and geochemical guide to the identification of hydrothermal monazite: criteria for selection of samples for dating epigenetic hydrothermal ore deposits. Economic Geology 99, 1027–1035.

Schmidt, C., Rickers, K., 2003. In-situ determination of mineral solubilities in fluids using a hydrothermal diamond-anvil cell and SR-XRF: solubility of AgCl in water. American Mineralogist 88, 288–292.

Schmidt, C., Rickers, K., Bilderback, D.H., Huang, R., Falkenberg, G., 2003. In situ determination of mineral solubilities using a diamond-anvil cell and SR-XRF: advantages of applying a single bounce capillary. Hasylab Annual Report, pp. 1143–1144.

Seydoux-Guillaume, A.-M., Paquette, J.-L., Wiedenbeck, M., Montel, J.-M., Heinrich, W., 2002. Experimental resetting of the U–Th–Pb systems in monazite. Chemical Geology 191, 165–181.

Seydoux-Guillaume, A.-M., Goncalves, P., Wirth, R., Deutsch, A., 2003. Transmission electron microprobe study of polyphase and discordant monazites: site-specific specimen preparation using the focused ion beam technique. Geology 31, 973–976.

Sharygin, A.V., Wood, R.H., 1997. Volumes and heat capacities of aqueous solutions of hydrochloric acid at temperatures from 298.15 K to 623 K and pressures to 28 MPa. Journal of Chemical Thermodynamics 29, 125–148.

Sobol', V.N., Puchkov, L.V., Zarembo, V.I., 1991. Volumetric properties (compression) of aqueous solutions of sodium metaborate and boric, sulfuric, and hydrochloric acid. Geokhimiya 9, 1349–1352 (in Russian).

Suominen, V., 1991. The chronostratigraphy of Southwestern Finland with special reference to Postjotnian and Subjotnian diabases. Geological Survey of Finland, Bulletin 356 (100 pp.).

Tagirov, B.R., Zotov, A.V., Akinfiev, N.N., 1997. Experimental study of dissociation of HCl from 350 to 500 °C and from 500 to 2500 bars: Thermodynamic properties of HCl° (aq). Geochimica et Cosmochimica Acta 61, 4267–4280.

Teufel, S., Heinrich, W., 1997. Partial resetting of the U–Pb system in monazite through hydrothermal experiments: an SEM and U–Pb isotope study. Chemical Geology 137, 273–281.

Van Espen, P., Janssens, K., Nobels, J., 1986. AXIL-PC, software for the analysis of complex X-ray spectra. Chemometrics and Intelligent Laboratory Systems 1, 109–114.

Vekemans, B., Janssens, K., Vincze, L., Adams, F., Van Espen, P., 1995. Comparison of several background compensation methods useful for evaluation of energy-dispersive X-ray fluorescence spectra. Spectrochimica Acta, Part B: Atomic Spectroscopy 50, 149–169.

Vincze, L., Janssens, K., Adams, F., 1993. A general Monte-Carlo simulation of ED-XRF spectrometers — I: unpolarized radiation, homogeneous samples. Spectrochimica Acta, Part B: Atomic Spectroscopy 48, 553–573.

Vincze, L., Janssens, K., Adams, F., Rivers, M.L., Jones, K.W., 1995a. A general Monte-Carlo simulation of ED-XRF spectrometers. II: polarized monochromatic radiation, homogeneous samples. Spectrochimica Acta, Part B: Atomic Spectroscopy 50, 127–147.

Vincze, L., Janssens, K., Adams, F., Jones, K.W., 1995b. A general Monte-Carlo simulation of energy dispersive X-ray fluorescence spectrometers. Part 3. Polarized polychromatic radiation, homogeneous samples. Spectrochimica Acta, Part B: Atomic Spectroscopy 50, 1481–1500.

Wagner, W., Saul, A., Pruβ, A., 1994. International equations for the pressure along the melting and along the sublimation curve of ordinary water substance. Journal of Physical and Chemical Reference Data 23, 515–527.

Walther, J.V., Orville, P.M., 1983. The extraction-quench technique for determination of the thermodynamic properties of solute complexes: application to quartz solubility in fluid mixtures. American Mineralogist 68, 731–741.

Wolf, A.V., Brown, M.G., Prentiss, P.G., 1981. Concentrative properties of aqueous solutions: conversion tables. In: Weast, R.C. (Ed.), CRC Handbook of Chemistry and Physics. CRC Press, pp. D198–D247.